Article

Analysis of the Mechanical Properties of a Bidirectional Laminated Slab with Shear Keys

Ming Li [1], Zhijun Zhou [1,*], Qian Wu [1,*], Wei Yan [1] and Shuang Yuan [2]

1 School of Civil Engineering, Shenyang Jianzhu University, Shenyang 110168, China
2 School of Construction Engineering, Tianjin University, Tianjin 300072, China
* Correspondence: me572742890@163.com (Z.Z.); 18624028257@163.com (Q.W.);
  Tel.: +86-024-24691800 (Q.W.)

Abstract: The load-bearing capacity of a bidirectional laminated slab with shear keys arranged in a rectangular grid (BCSWSK) was investigated to determine its mechanical properties, using load tests on a fabricated laminated slab and finite element models. The shear force distribution across the shear keys was measured and analysed, and the effects of different parameters were identified. The interfaces between the cast bottom slab and the shear keys were strongly bonded, as was the interface between the precast bottom slab and the cast-in-place upper slab, despite it being a secondary concrete pouring. The shear force was distributed similarly along the X direction (columns) and the Y direction (rows) of the shear key arrangement. The shear forces along the Y direction were greater and reached a maximum value sooner, but the differences between columns were mostly less than 10%. A square cross-section is recommended for the shear keys. The number of rows, number of columns, and the cross-sectional area of the shear keys are the main factors influencing the mechanical properties of the composite slab, but as they individually increased, they reached a point at which further increase had little effect. Similarly, after a certain number of shear keys were used, the concrete grade cast in situ, the shear key concrete grade, and the friction coefficient between the precast bottom slab and the cast-in-place upper slab had little influence on the BCSWSK.

Keywords: laminated slab and plates; composite slab and plates; shear key; influencing factor; element modelling

1. Introduction

A laminated concrete slab consists of a prefabricated bottom slab (PBS) and a cast-in-place concrete upper slab (CCUS). Its advantages over conventional cast-in-place slabs are ease of construction, green and low-carbon technology, and high-production efficiency. It is an important horizontal load-bearing member of assembled concrete structures and has been widely used in housing construction [1]. The most commonly used forms of laminated slabs are steel-truss-laminated slabs (STLSs) (Figure 1a) and ribbed laminated slabs (RLSs) (Figure 1b). Of which, the steel truss is made automatically by machine. An in-depth study shows that, in conjunction with the wider uses of STLSs, the increased use of steel reinforcement in them leads to greater slab thickness [2], resulting in higher construction costs. The ribs of RLSs extend for the full length of the slab, which can be problematic in crossing pipelines. Furthermore, the PBSs of them must be temporarily supported during construction due to their limited stiffness. To overcome the problems associated with the use of these types of laminated slabs, a concrete-laminated slab with shear keys (CSWSK) was proposed to connect the PBS to the CCUS (Figure 2a). The shear keys can also be connected to temporary I-beams to increase the stiffness of the PBSs to realise support-free construction (Figure 2b).
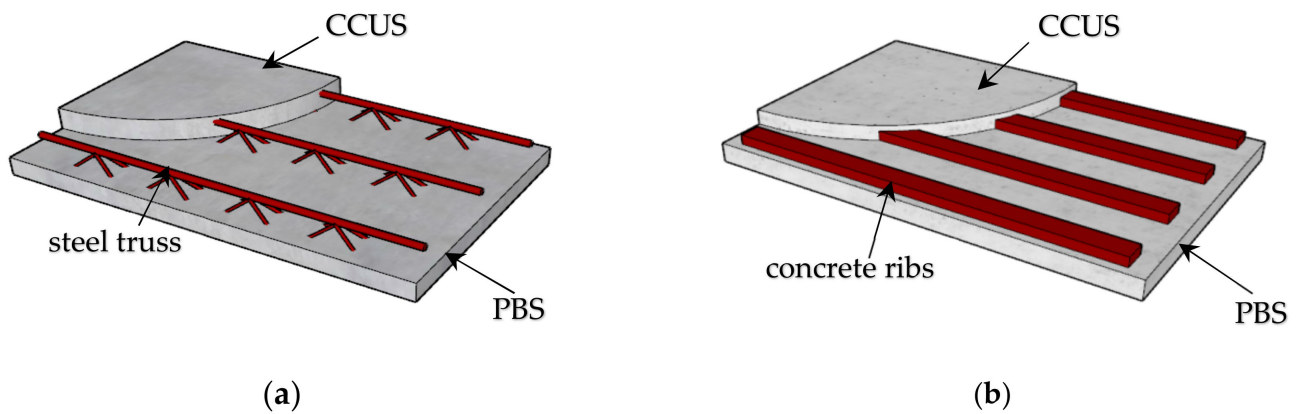
Figure 1. The most commonly used forms of laminated slab: (**a**) STLS; (**b**) RLS.
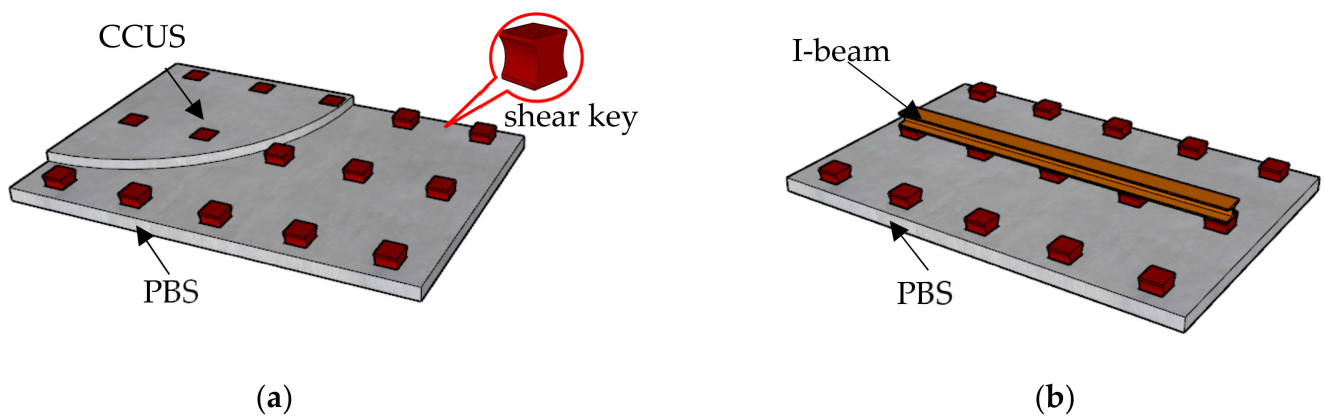

Figure 2. CSWSK and precast bottom slab with I-beam bolted to it: (**a**) CSWSK; (**b**) PBS with I-beams bolted to it.

There are large bodies of systematic research on each [3–11]. Liu et al. [12] confirmed the practicality of using STLSs by empirical testing; Ma et al. [13] investigated its mechanical properties in construction and in service by testing and numerical modelling; Zhao et al. [14] analysed the influence of parameters, such as concrete strength and truss height and diameter, on the mechanical properties of STLSs using ANSYS software; and Cheng [15] developed a short-term stiffness model for STLSs from theoretical analysis. Wu et al. [16] confirmed the practicality of using RLSs by empirical testing; Qian et al. [17] experimentally investigated its mechanical properties, such as the flexural-bearing capacity and the shear resistance of the laminated surface, in construction and in service; Shi et al. [18] analysed the effects of parameters, such as rib height, and rib width and reinforcement rate, on the mechanical properties of RLSs using a finite element method and experimental testing; and Huang et al. [19] developed deflection and bending moment equations for RLSs in service, using load superposition and an orthotropic and anisotropic plate theory. However, for CSWSKs, only we have conducted a series of studies on its unidirectional mechanical properties [20,21], and this paper continues that series by investigating the mechanical properties of bidirectional laminated slabs with shear keys (BCSWSKs), including the flexural-bearing capacity, damage modes, and influencing factors, using experimental tests and finite element modelling. A flowchart of this study is shown in Figure 3.
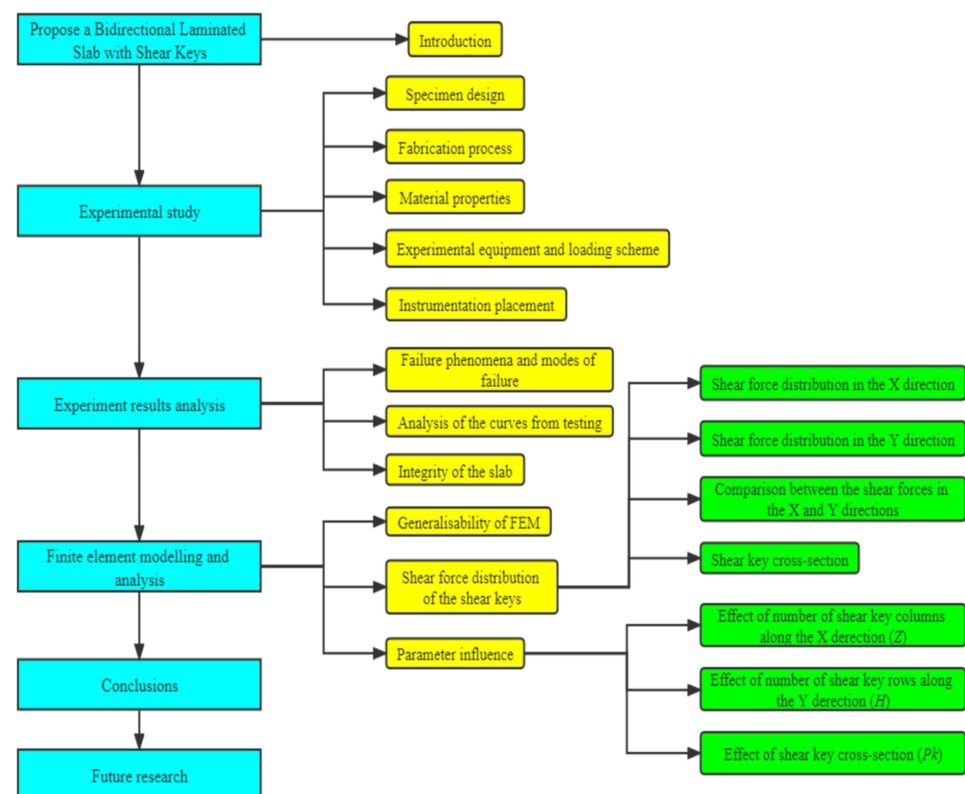
Figure 3. Flowchart of this study.

2. Experimental Study

One BCSWSK was designed and fabricated, according to standards GB (50010-2010) [22] and JGJ (1-2014) [23], to be incorporated into an existing structure. The shear keys were designed according to finite element modelling, of which the generalisability was not verified. It was tested in the Civil Engineering Structure Test Centre (Shenyang, China) of Shenyang Jianzhu University.

2.1. Specimen Design

The dimensions and form of the shear keys used in the BCSWSK are shown in Figure 4. The vertical faces were concave arcs, and the top and bottom faces were flat. The concave arc faces were designed to prevent the PBS and the CCUS from separating in the direction perpendicular to them. The concrete grade of the PBS and the CCUS was C25, and the depth/thickness of each was 50 mm. The concrete grade of the shear keys was C30: this was greater than the strength of the two slabs to prevent the keys from failing before the slab failed. The PBS is shown in Figure 5. The reinforcements had a diameter = 8 mm and tensile yield strength = 335 MPa. Field curing was adopted for the specimen.
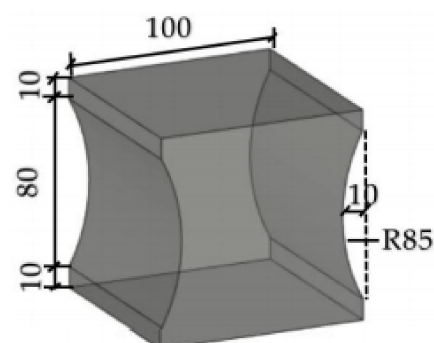

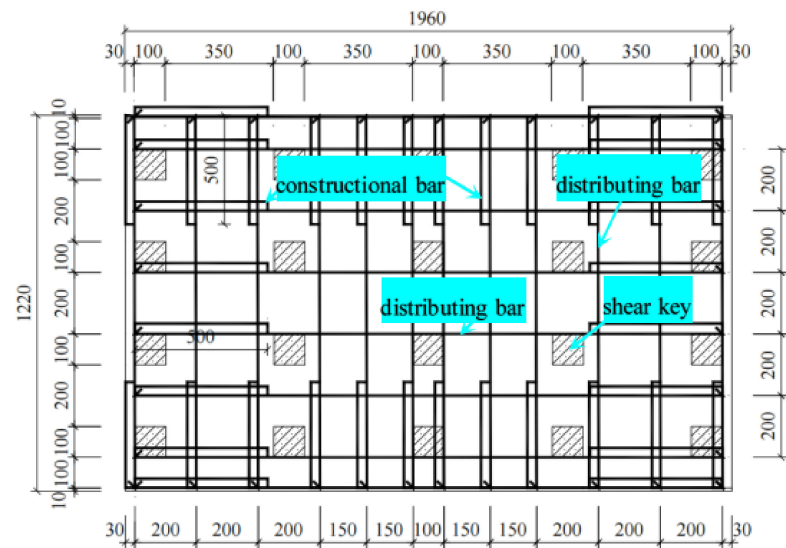**Figure 4.** Dimensions and shape of shear key.

Figure 5. PBS of BCSWSK.

2.2. Fabrication Process

The fabrication process of the BCSWSK was as follows. The shear keys were made by cutting a long columnar concrete strip. The steel-reinforcing bars and shear keys were positioned in the mould, and concrete was poured to form the precast bottom slab (Figure 6a). After 28 days, the concrete of the CCUS was poured on top of the PBS to complete the lamination. The finished BCSWSK is shown in Figure 6b.

(a) (b)
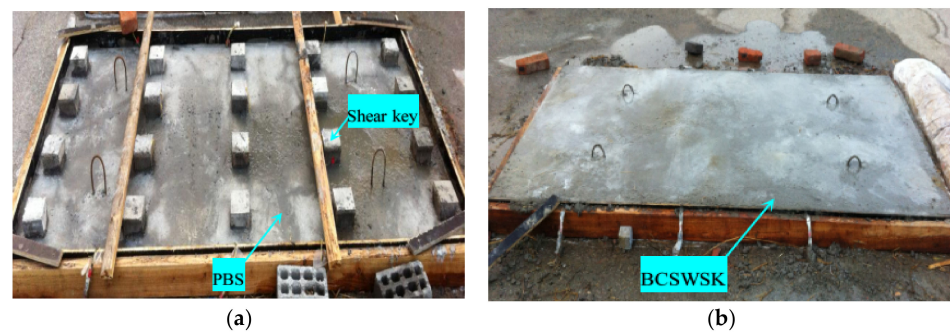
Figure 6. The production process for BCSWSK: (**a**) Precast bottom slab of BCSWSK; (**b**) BCSWSK.

2.3. Material Properties

The material properties of the steel bar and concrete were tested separately in the test rigs shown in Figure 7a,b. The compressive strength of the concrete (f_{ck}), the yield strength of the steel bar (f_y), the ultimate strength of the steel bar (f_u), and the corresponding Young's modulus ($E_c(E_s)$) are shown in Table 1.

(a) (b)

Figure 7. Steel bar and concrete materials tests: (**a**) Test rig for tensile strength of steel bar (HRB335); (**b**) Test rig for compressive strength of concrete.

Table 1. Measured mechanical property indexes of concrete and steel bar.

| Batch	Material	f_{ck} (MPa)	f_y (MPa)	f_u (MPa)	$E_c(E_s)$ (MPa)
Precast bottom slab	Concrete	21.4	–	–	2.80×10^4
Post pouring concrete	Concrete	26.8	–	–	2.80×10^4
Shear keys	Concrete	27.6	–	–	3.00×10^4
HRB335	Steel bar	–	350	460	2.0×10^5

2.4. Experimental Equipment and Loading Scheme

The testing used a combination of sandbag loading and jack loading; the concentrated load exerted by the jack was transmitted to the slab by the sandbags. The loading device is shown in Figure 8. The slab was supported as follows. Two adjacent sides of the slab were supported by the immovable hinges of a triangular steel pipe, and the other two adjacent sides were supported by the rolling hinges of a cylindrical steel pipe. A steel slab was set between the bottom of the precast concrete slab and the hinge supports to avoid local compression failure. Seven layers of sandbags were stacked on the top slab surface, with eight bags per layer and each sandbag weighing 25 kg. A load-transfer device was placed on top of the sandbags. A jack was applied to the steel mat to apply the test load. For the loading system, the initial, maximum, and final settlement values were 0, 500, and 199 kN.
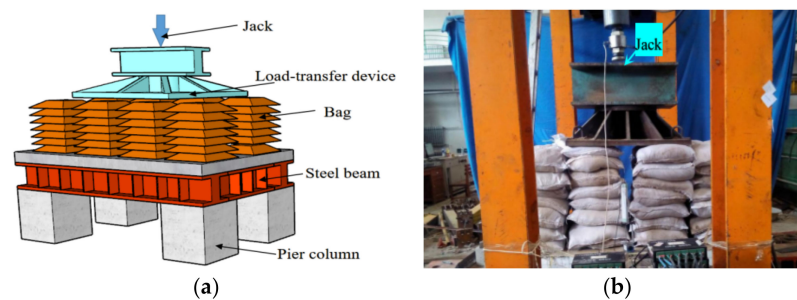
Figure 8. Loading system: (**a**) Schematic; (**b**) Photo.

2.5. Instrumentation Placement

Five displacement meters designated W1 to W5 were arranged symmetrically at the midpoints and the quarter points of the length and width of the slab bottom to measure the vertical displacement of the BCSWSK under vertical load. Strain gauges designated Y1 to Y12 were attached close to the midpoint and quarter points of the reinforcement to measure the strain of the tensile reinforcement at the bottom of the slab (Figure 9a). Displacement gauges designated W6 and W7 were arranged at the centre of the precast and laminated slabs to measure the relative displacement between the precast bottom slab and the cast-in-place concrete (Figure 9b).
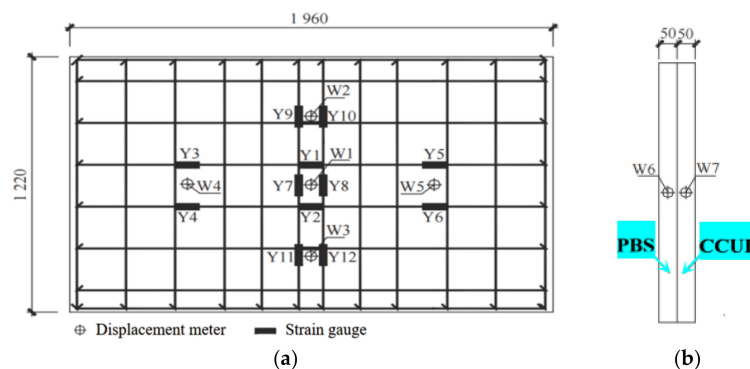
Figure 9. Placement of displacement meters and strain gauges for BCSWSK testing: (**a**) Placement of displacement meters and strain gauges at the bottom of the slab; (**b**) Placement of displacement meters at the centre of the slab.

3. Test Results

3.1. Failure Phenomena and Modes of Failure

The failure process of the BCSWSK was as follows. The first crack appeared on the side of the specimen when it was loaded to 80 kN; it was roughly vertical. When loaded to 160 kN, the cracks on the side of the slab extended to the slab bottom and developed to the mid-span. When loaded to the measured ultimate load (213 kN), destructive deformation occurred. The maximum crack appeared at the mid-span, where the crack width exceeded 1.5 mm, and the number of cracks also began to increase, indicating that the slab had failed (Figure 10).
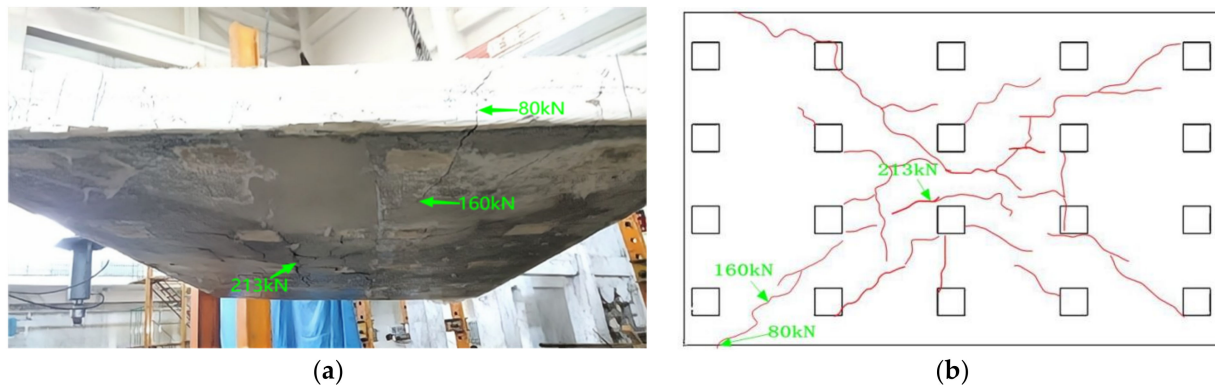

(**a**)   (**b**)

Figure 10. Crack patterns of BCSWSK after testing: (**a**) Photo; (**b**) Maps of failure patterns.

3.2. Analysis of the Curves from Testing

The load–strain curve of the tensile steel bar is shown in Figure 11, and the load–displacement curve of the concrete at the mid-span is shown in Figure 12.

It can be seen from the load–strain curve of the tensile-reinforcement steel bar of the BCSWSK (Figure 11) that, before the first crack occurred, the increase in load was approximately linearly proportional to the change in strain of the tensile steel bar, and the strain values were relatively small. As the load increased until cracks appeared in the specimen, the strain of the tensile reinforcement increased significantly, and there was a turning point in the curve. When the load increased to 160 kN, the tensile steel bar yielded, and the strain of the steel bar reached the yield value. It can be seen from Figure 12 that the load–displacement curve of the BCSWSK included an elastic section, an ascending inelastic section, and no descending section. The behaviour is similar to that of the cast-in-place slab, which indicates the integrity of the lamination [24].
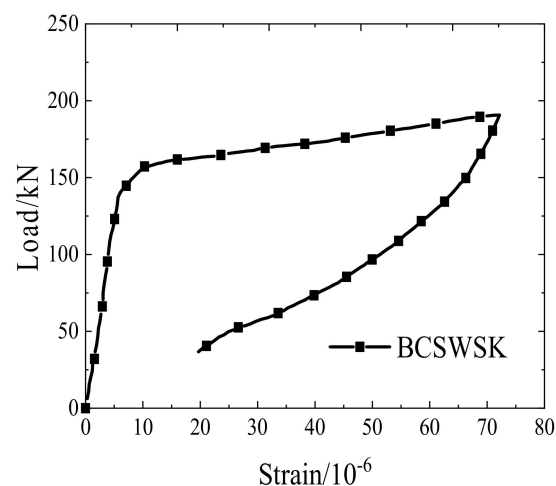

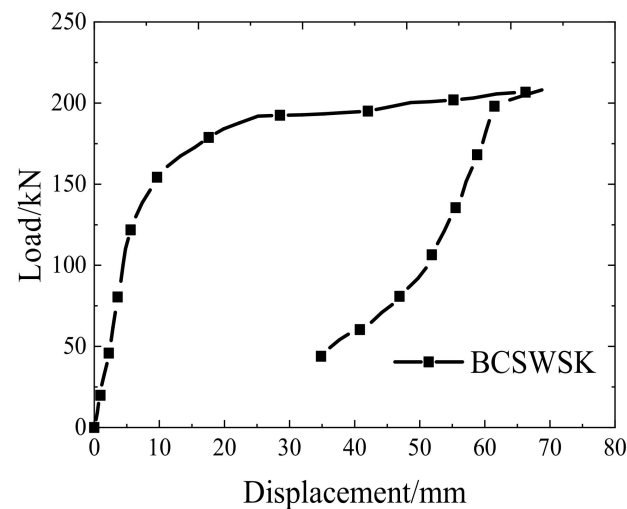**Figure 11.** Load–strain curve of the tensile steel bar at mid-span.

Figure 12. Load–displacement curve of the laminated concrete at mid-span.

3.3. Integrity of the Slab

In the fabrication of the BCSWSK, 28 d after the initial cast, there was a second concrete pour of the laminated slab, introducing concrete above the PBS and between the shear keys. Analysing the strength of the connection between the two was a key objective of the experiment. There was no disconnective cracking at the interfaces of the precast slab and the shear keys, which indicates that the precast slab and the shear keys were firmly connected and well-integrated (Figure 13). The horizontal displacement gauges (W6 and W7) showed that the relative displacement of the two slabs was almost zero, which also indicates the integrity of the PBS and the CCUL. It can also be seen that the crack pattern presents the failure characteristics of a two-way slab, which further shows its good integrity.

Figure 13. Failure of the precast bottom slab.

4. Finite Element Modelling and Analysis

Although the experimental results provide valuable information, they are limited to the material studied. Finite element analysis was used to generalise the results of the study. The main objectives of the numerical analysis were: (1) to determine the generalisability of the finite element model (FEM); (2) to determine the shear force distribution of the shear keys; and (3) to determine the effects of the main influencing parameters of the mechanical behaviour of the BCSWSK.

4.1. Generalisability of FEM

The load-bearing behaviour of the laminated concrete slab was modelled using ABAQUS. A concrete plastic-damage (CPD) model [24] was adopted for the constitutive relations of concrete. The equation of the compressive σ–ε curve used for it is:

$$\sigma_c = \begin{cases} \dfrac{E_c{}^2 f_{c.r}\varepsilon}{\dfrac{E_c{}^2\varepsilon_{c.r}}{\left(E_c{}^2\varepsilon_{c.r}-f_{c.r}\right)^2}-\left(\varepsilon_{c.r}E_c{}^3\varepsilon-E_c f_{c.r}\varepsilon\right)\left[1+\left(\frac{\varepsilon}{\varepsilon_{t.r}}\right)^{\frac{E_c\varepsilon_{c.r}}{E_c\varepsilon_{c.r}-f_{c.r}}}\right]} \\[3em] \dfrac{f_{c.r}\varepsilon}{\varepsilon_{c.r}E_c\varepsilon\left[\left(0.157 f_{c.r}^{0.785}-0.905\right)\left(\frac{\varepsilon}{\varepsilon_{t.r}}-1\right)^2+\frac{\varepsilon}{\varepsilon_{t.r}}\right]} \end{cases} \tag{1}$$

$$\varepsilon_{c.r}=\left(700+175\sqrt{f_c}\right)\times 10^{-6} \tag{2}$$

where $f_{c,r}$ is the representative value of concrete, $\varepsilon_{c,r}$ is the corresponding strain, E_c is the damage evolution parameters, and f_c is the standard compressive strength of the concrete.

A bifold model [25] was adopted for the constitutive relations of reinforcement. The equation of the σ–ε curve used for it is:

$$\sigma = \begin{cases} E\varepsilon & \varepsilon \le \varepsilon_y \\ f_y+0.01E(\varepsilon-\varepsilon_y) & \varepsilon > \varepsilon_y \end{cases} \tag{3}$$

where f_y is the yield strength of steel bar and ε_y is the corresponding strain.

The PBS, shear keys, and CCUL were all C3D8R elements, and the steel bar was a T3D2 element incorporated into the concrete as an embedded region. The boundary conditions, loading modes, and meshing of the model are shown in Figure 14. The interface between the PBS and the CCUL was friction contact. The Newton iterative method was used to solve the FEM equations.

(**a**)　　　　　　　　　　　　　　　　　　　(**b**)

(**c**)
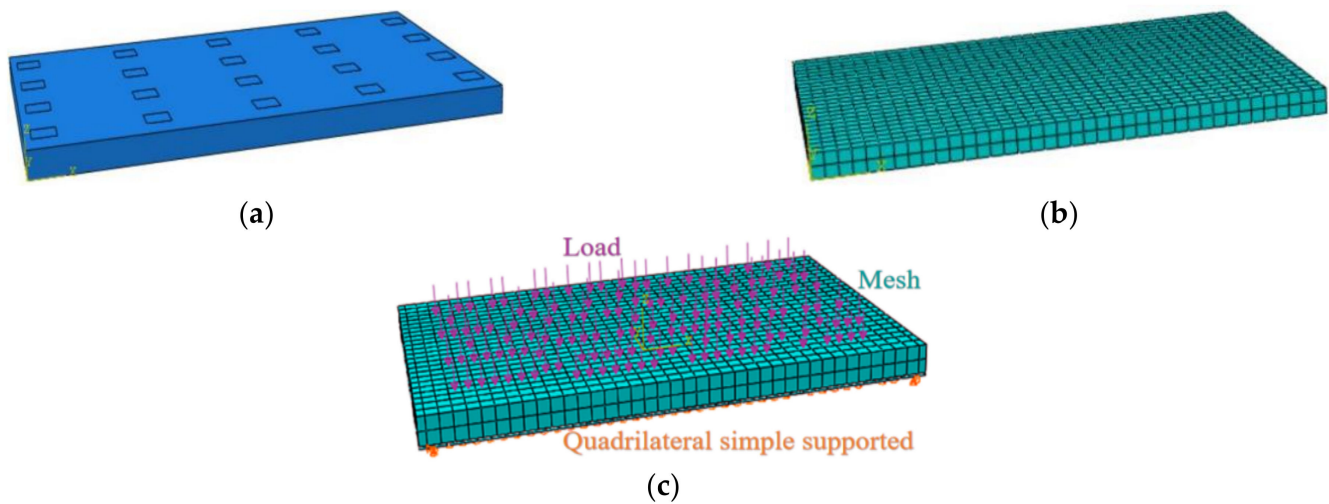
Figure 14. Boundary conditions, loading, and mesh generation of the model: (**a**) Unmeshed; (**b**) Load mesh preparation; (**c**) Load mesh.

The load–displacement curves and the load–strain curves of the reinforcement given by the FEM were compared with the test results (Figure 15). It can be seen that the simulated curve and the test curve were almost identical; the maximum difference was <1.5%, thus verifying the generalisability of the FEM.
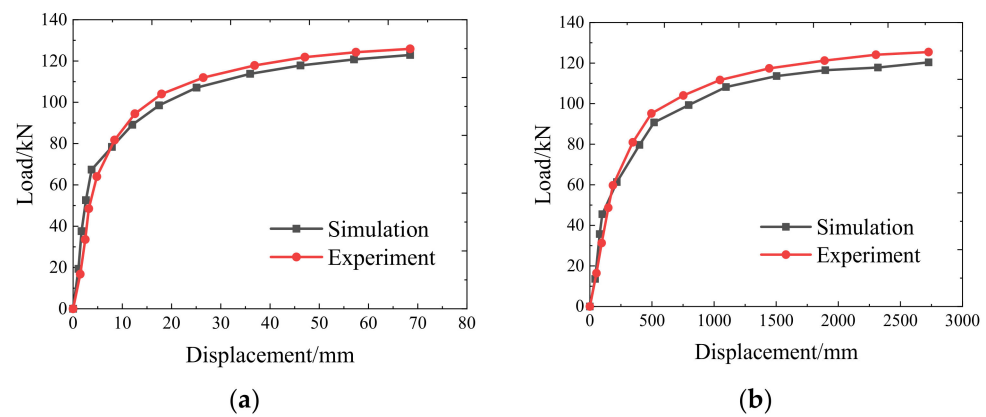
Figure 15. ABAQUS model and experimental results for comparison: (**a**) Load–displacement curves at mid-span; (**b**) Load–strain curves of steel bars.

4.2. Shear Force Distribution of the Shear Keys

Under vertical load, there was a relative misalignment between the PBS and the CCUL of the BCSWSK, which produced shear force in the shear keys. There were some differences between the keys in shear force along both the X and Y directions. A BCSWSK FEM, designated FJ1, was designed to enable us to analyse the shear distribution among the shear keys. The slab was grade C25 concrete, and the shear keys were grade C30. The remaining dimensions and physical parameters were identical to those of the test specimen. An identical loading process was simulated.

The shear force distribution within FJ1 under uniform vertical load was the same as for the original cast specimen because of the same symmetrical distribution of the shear keys along the X and Y directions. The shear keys in a quarter of the area of the slab were therefore selected for analysis, and they were numbered for convenience of description, as shown in Figure 16a.
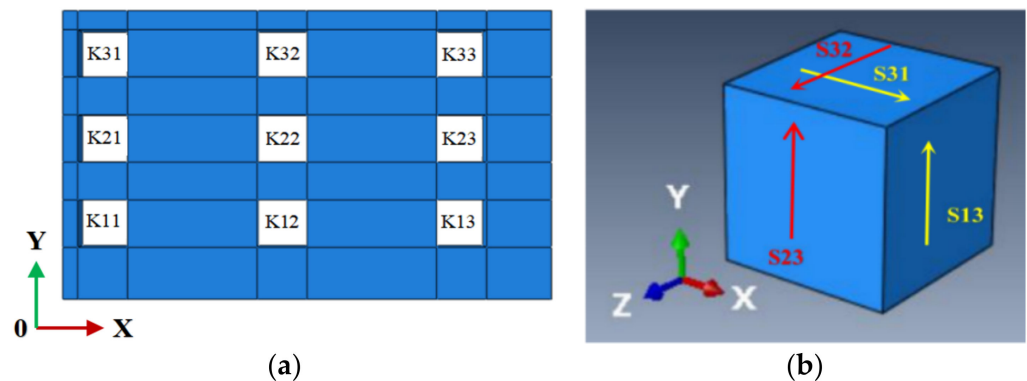

Figure 16. Number of shear keys and shear stress directions: (**a**) Number of shear keys in the quarter area of FJ1; (**b**) Shear stress directions on one shear key.

The shear keys were divided into eight elements. The shear stress directions of an element are shown in Figure 16b. X and Y are the length and width directions of FJ1, respectively. S13 is the shear stress along the Z direction in the YZ plane, and S23 is the shear stress along the Z direction in the XZ plane. According to the reciprocal theorem for shear stresses in the vertical plane, S31 = S13 and S32 = S23. The total shear force of a shear key at the contact surface of the PBS and the CCUL of FJ1 can be obtained: its value along the X direction is the product of S31 and its cross-sectional area, and its value along the Y direction is the product of S32 and its cross-sectional area. The relationship between the total load applied to FJ1, and the total shear force of each shear key in the X direction and the Y direction, can be plotted, as shown in Figure 17 (X) and Figure 18 (Y).
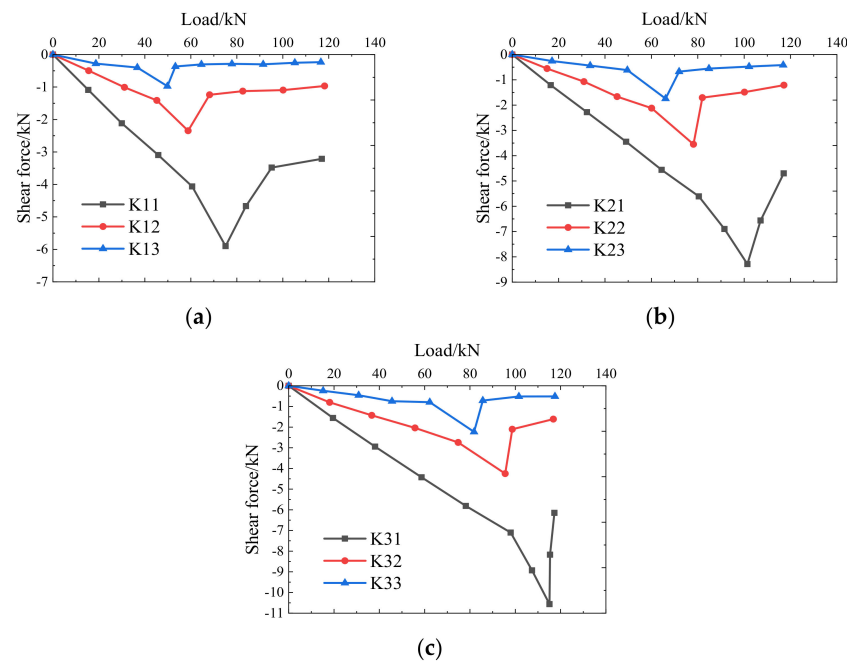
Figure 17. Load–shear force curves of the three groups of shear keys along the X direction: (**a**) K11–K13; (**b**) K21–K23; (**c**) K31–K33.
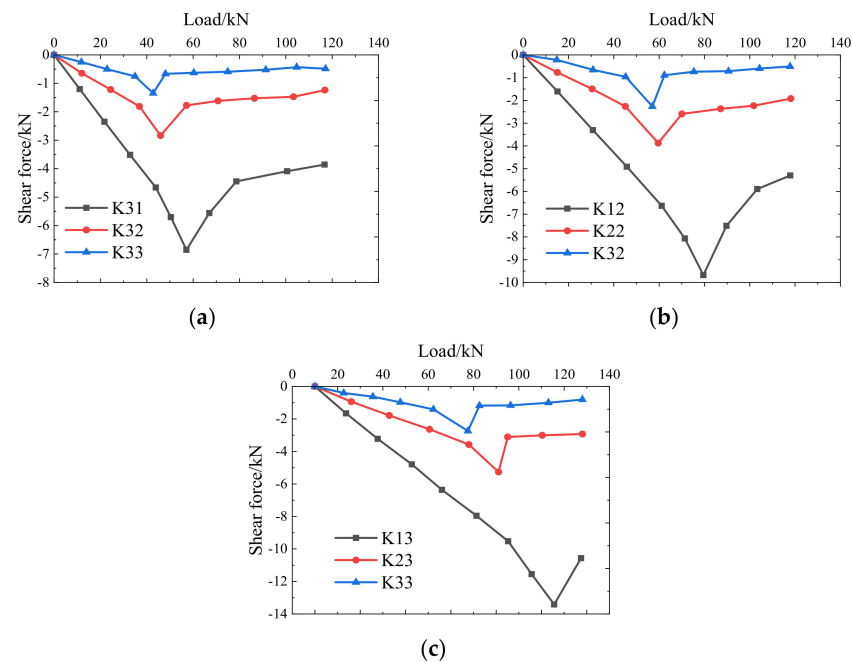
Figure 18. Load–shear force curves of the three groups of shear keys in the Y direction: (**a**) K11–K31; (**b**) K12–K32; (**c**) K13–K33.

4.2.1. Shear Distribution in the X Direction

Figure 17 shows the load–shear force curves of shear keys K11–K13, K21–K23, and K31–K33. It can be seen that for, all three groups of shear keys, the shear force increased linearly as the vertical load increased, and suddenly decreased when the shear force reached a maximum value. This behaviour indicates that the failure was brittle. The maximum shear force differed between the three groups: it was lowest near the mid-span and highest near the support. This is because the shear keys near the mid-span were primarily affected by bending moments. The vertical loads were different when the shear force reached its maximum value, so the shear keys did not all fail at the same time. As

the vertical load increased, failure gradually developed from the shear keys in the region with a larger bending moment near the mid-span, to the supported region with a smaller bending moment.

A comparison of the maximum shear force between the three groups of shear keys shows that, although the load–shear curves of the three groups were very similar, the shear values of K31–K33 were the greatest, and the shear values of K21–K23 and K11–K13 were the least. This was mainly because, under a vertical uniform load, FJ1 deformed along the diagonal in the area nearest the support. Deformation increased towards the centre of the slab, as did the misalignment between the precast bottom slab and the cast-in-place slab. The group of shear keys K31–K33 was closest to the centre of the slab, so resistance to the shear force generated by the misalignment was greatest for this group.

4.2.2. Shear Force Distribution in the Y Direction

The load–shear force curves for the three groups of shear keys K11–K31, K12–K32, and K13–K33, in the Y direction of FJ1, are shown in Figure 18. It can be seen that, similar to the X direction, the shear force increased linearly as the applied vertical load increased and suddenly decreased when it reached a maximum value. In each of the three groups of shear keys, the shear force was at a maximum near the support and at a minimum near the mid-span of the slab. In each group, the load values differed when the shear force reached the maximum value. A comparison of the maximum shear values shows that the shear resistance of K13–K33 was greatest because they were close to the centre of the slab.

4.2.3. Comparison between the Shear Forces in the X and Y Directions

Figure 19 shows the load–shear force curves of K11, K22, and K33 in the X and Y directions. It can be seen that the maximum shear force was greater in the Y direction than in the X direction, and that the shear force in the Y direction reached the maximum value first. This is because the bending moment of FJ1 was greater in the short-span direction than in the long-span direction, and so the bending moment had a greater effect on the shear force of the keys in the Y direction. Thus, it would be better to give the shear keys a rectangular cross-section with the longer side parallel to the short span when designing a BCSWSK to make them more effective in resisting shear.
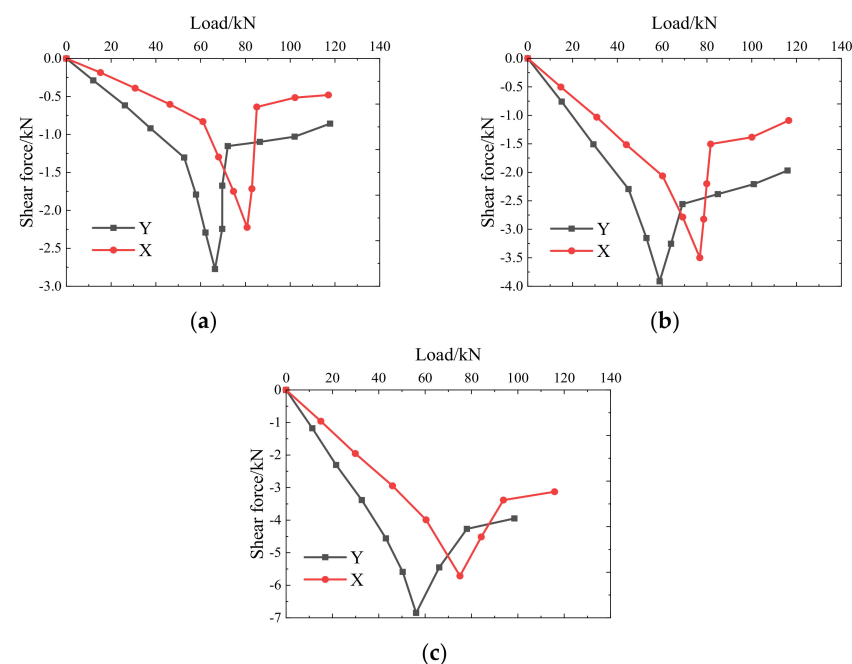

Figure 19. Load–shear force curves of different shear keys along the X and Y directions for comparison: (**a**) K11 along the X and Y directions; (**b**) K22 along the X and Y directions; (**c**) K33 along the X and Y directions.

4.2.4. Shear Key Cross-Section

The preceding analysis indicates that a rectangular shear key cross-section would be better than a square cross-section in terms of resisting shear. To clarify this issue, rectangular cross-section shear keys with different dimensions were modelled in the FEM. Figure 20 shows the different load–displacement curves obtained for the keys with respective dimensions in the X and Y directions: (L_{XY}) 50 × 200 mm, 100 × 100 mm, and 200 × 50 mm. Other dimensions and physical parameters were identical to those of FJ1. It can be seen that the bearing capacity was greatest for the 50 × 200 mm key until the displacement was about 53 mm, but after this point, the bearing capacity became greatest for the 200 × 50 mm key. However, the difference between the three curves was slight, mostly <10%, so the square cross-section is recommended for the shear keys.
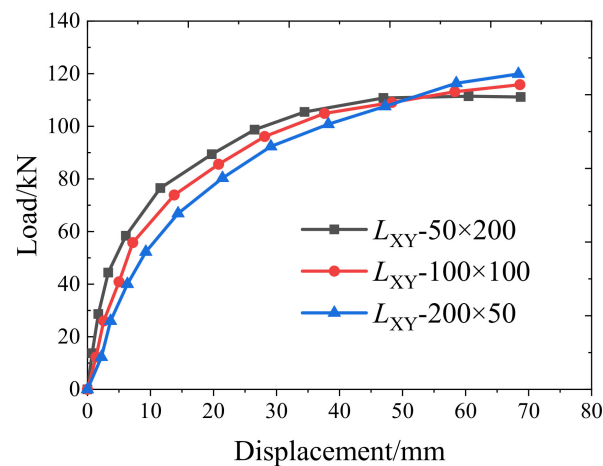

Figure 20. Load–displacement curves of BCSWSKs with different shear-key shapes for comparison.

4.3. Parameter Influence

Twenty-five laminated slabs were modelled to allow us to analyse the influence of different factors on the load–displacement curves of BCSWSKs, as shown in Table 2. All dimensions and physical parameters were identical to those of model FJ1, except for the parameters that were varied experimentally. The simulations show that changing the friction coefficient, the grade of the cast-in-place concrete, and the grade of the concrete used with shear keys had very little effect on the mechanical properties of BCSWSKs, mostly <3.2%, and their load–displacement curves almost coincided, but changing the other parameters had clearly observable effects, as shown in Figures 21–23.
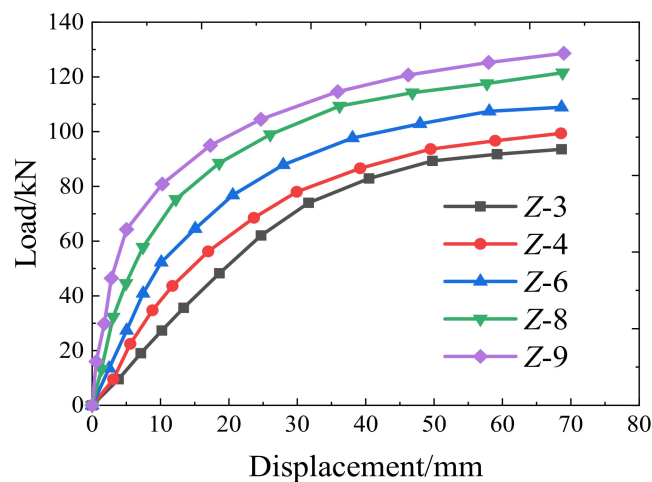

Figure 21. Load–displacement curves of BCSWSKs with different numbers of columns of shear keys for comparison.
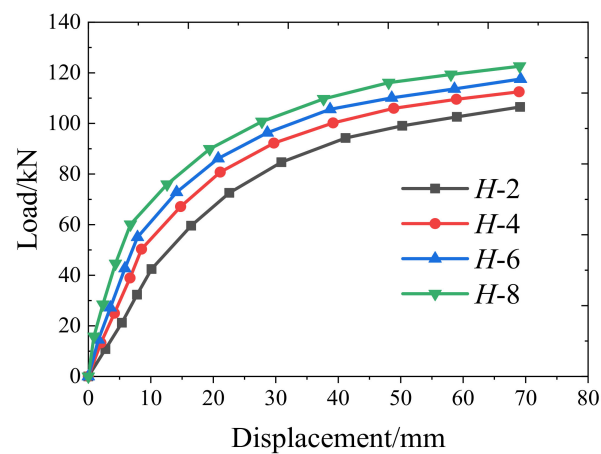
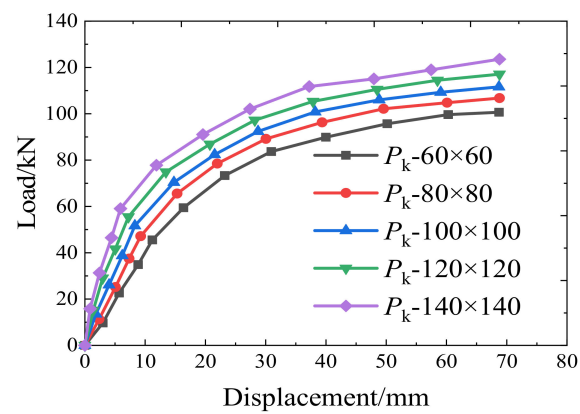**Figure 22.** Load–displacement curves of BCSWSKs with different numbers of rows of shear keys for comparison.

Figure 23. Load–displacement curves of BCSWSKs with different shear key dimensions for comparison.

Table 2. List of laminated slabs modelled.

Model Designation	Number of Shear Key Columns Z	Number of Shear Key Rows H	Shear Key Cross-Section Dimensions P_k (mm)	Concrete Grade		Friction Coefficient f	Yield Load (kN)	Yield Displacement (mm)
				Cast-in-Place Concrete S_i	Shear key S_k			
f-0	6	4	100 × 100	C25	C30	0	77.2	16.7
f-0.4	6	4	100 × 100	C25	C30	0.4	77.4	16.6
f-0.6	6	4	100 × 100	C25	C30	0.6	77.8	16.4
f-0.8	6	4	100 × 100	C25	C30	0.8	78.3	16.2
S_i-20	6	4	100 × 100	C20	C30	0.8	77.5	16.0
S_i-25	6	4	100 × 100	C25	C30	0.8	78.3	16.2
S_i-35	6	4	100 × 100	C35	C30	0.8	79.3	16.5
S_k-20	6	4	100 × 100	C25	C20	0.8	77.9	16.4
S_k-30	6	4	100 × 100	C25	C30	0.8	78.3	16.2
S_k-40	6	4	100 × 100	C25	C40	0.8	78.9	16.0
Z-3	3	4	100 × 100	C25	C30	0.8	70.4	23.5
Z-4	4	4	100 × 100	C25	C30	0.8	74.7	19.4
Z-6	6	4	100 × 100	C25	C30	0.8	78.3	16.2
Z-8	8	4	100 × 100	C25	C30	0.8	80.7	14.0
Z-9	9	4	100 × 100	C25	C30	0.8	81.7	12.5
H-2	6	2	100 × 100	C25	C30	0.8	72.4	22.4
H-4	6	4	100 × 100	C25	C30	0.8	75.7	18.2
H-6	6	6	100 × 100	C25	C30	0.8	78.3	16.2
H-8	6	8	100 × 100	C25	C30	0.8	79.5	15.0
P_k-60 × 60	6	4	60 × 60	C25	C30	0.8	70.6	23.2
P_k-80 × 80	6	4	80 × 80	C25	C30	0.8	75.4	18.8
P_k-100 × 100	6	4	100 × 100	C25	C30	0.8	78.3	16.2
P_k-120 × 120	6	4	120 × 120	C25	C30	0.8	79.6	15.3
P_k-140 × 140	6	4	140 × 140	C25	C30	0.8	81.0	13.0

4.3.1. Effect of Number of Shear Key Columns along the X Direction (*Z*)

Figure 21 shows the load–displacement curves of BCSWSKs for different numbers of shear key columns (*Z* = 3, 4, 6, 8, 9). Figure 21 and Table 2 show that the bearing capacity increased as the number of shear key columns increased. When the number of columns increased from three to nine, the yield load increased by 16.1% and the yield displacement decreased by 47%. When the number of columns increased from eight to nine, the yield load increased by 1.2% and the yield displacement decreased by 10.8%. These results show that increasing the number of columns increases the yield load and decreases the yield displacement of the BCSWSK, but this trend is not so pronounced after a certain point. This reduction in effectiveness occurs because, at some point, the number of shear keys in the slab is such that the relative misalignment between the PBS and the CCUL is very small, so increasing the number of shear keys has little effect.

4.3.2. Effect of Number of Shear Key Rows along the Y Direction (*H*)

Figure 22 shows the load–displacement curves of BCSWSKs for different numbers of rows of shear keys (*H* = 2, 4, 6, 8). Figure 22 and Table 2 show that the bearing capacity increased as the number of shear key rows increased. When the number of rows increased from two to eight, the yield load increased by 9.8% and the yield displacement decreased by 33.2%. When the number of rows increased from six to eight, the yield load increased by 1.5% and the yield displacement decreased by 7.5%. These results show that increasing the number of rows of shear keys increases the yield load and decreases the yield displacement of the BCSWSK, but this trend is not so pronounced after a certain point. The reason for this is the same as that for the increase in the number of columns. However, a change in the number of rows has a relatively small effect on the bearing capacity of BCSWSKs compared to a change in the number of columns.

4.3.3. Effect of Shear Key Cross-Section (*P_k*)

Figure 23 shows the load–displacement curves of the BCSWSK with different shear key cross-sections (*P_k* = 60 × 60, 80 × 80, 100 × 100, 120 × 120, and 140 × 140 mm). It can be seen from Figure 23 and Table 2 that bearing capacity increased as the shear key cross-section increased. When the cross-section increased from 60 × 60 mm to 140 × 140 mm, the yield load increased by 19.5% and the yield displacement decreased by 44%. When the cross-section increased from 120 × 120 mm to 140 × 140 mm, the yield load increased by 1.8% and the yield displacement decreased by 1.5%. These results show that increasing the cross-section areas of the shear keys increases yield load and decreases the yield displacement of BCSWSKs, but this trend is not so pronounced after a certain point. The reason for this is the same as that for the effect of the number of columns.

5. Conclusions

In this research, experimental testing and FEMs were used to analyse shear force distribution and the factors that influence the mechanical properties of BCSWSKs under the action of uniform vertical load. In view of the test results and analysis, the following conclusions can be drawn.

(1) The loading scheme of stacking and jacking to apply an equivalent uniform load is appropriate. The bonds at the interfaces between the PBS and the shear keys, and between the PBS and the CCUL, are strong despite the secondary concrete pouring for the upper slab.

(2) The shear force distribution among its shear keys is similar in the X and Y directions. The shear force increases linearly as the load increases and decreases suddenly when the load reaches a certain point, namely when the shear keys show brittle failure. The shear force is greater in the Y direction than in the X direction and reaches a maximum value earlier. The difference in shear force distribution among shear keys between the two directions is small, mostly <10%. A square cross-section is recommended for the shear keys.

(3) The number of rows, number of columns, and cross-sectional area of the shear keys are the main factors that influence the mechanical properties of BCSWSKs, of which the yield load and yield displacement varies by 9.8%~19.5% and 33.2%~47%, respectively. The effectiveness of all three factors decreases as the factors increase and, after a certain point, the effect is minimal, mostly <7.5%. After a certain number of shear keys have been placed, the cast-in-place concrete grade, the shear key concrete grade, and the friction coefficient between the precast bottom slab and the cast-in-place slab have little influence on the mechanical properties, mostly <3.2%.

6. Future Research

This study investigated the mechanical properties of BCSWSKs using load tests on a fabricated laminated slab and finite element models. The shear force distribution across the shear keys was measured and analysed, and the effects of different parameters were identified. These provide much reference for the design of BCSWSKs in the service stage. However, their mechanical properties in the construction stage was not studied, such as the bending properties of PBSs and PBSs with I-beams bolted to them. As such, more research should be conducted on them for their engineering practicality.

Author Contributions: Conceptualization, M.L. and Z.Z.; methodology, Z.Z.; software, W.Y.; validation and formal analysis, Z.Z.; data curation, S.Y.; writing—original draft preparation, M.L.; writing—review and editing, Q.W. All authors have read and agreed to the published version of the manuscript.

Institutional Review Board Statement: Not applicable.

Informed Consent Statement: Not applicable.

Data Availability Statement: The data used to support the findings of this study are available from the corresponding author upon request.

Conflicts of Interest: The authors declare no conflict of interest.

References

1. Xie, Q. Reflections on the development of assembled concrete structure buildings. *Eng. Constr. Des.* **2021**, *23*, 26–30. (In Chinese)
2. Nie, J.; Jiang, Y.; Nie, X.; Zhuang, L. Effect of truss reinforcement in laminated slabs on the force performance of precast slabs. *J. Build. Struct.* **2021**, *42*, 151–158. (In Chinese)
3. Liu, W.; Cui, S.; Liu, C.; Shi, L. Experimental and theoretical study on the flexural performance of prestressed concrete steel truss laminated slabs. *J. Build. Struct.* **2021**, *42*, 95–106. (In Chinese)
4. Yang, X.; Wang, Y.; Liu, Y.; Wei, Z. Experimental Study and Numerical Simulation on Mechanical Properties of the Bottom Plate in the Assembled Composite Slab with Additional Steel Trusses. *Adv. Civ. Eng.* **2021**, *2021*, 7240994. [CrossRef]
5. Kanchanadevi, A.K.; Ramanjaneyulu, K.; Srinivas, V. Behaviour of concrete composite slabs with truss type shear connectors of different orientation angle. *Adv. Struct. Eng.* **2021**, *24*, 3070–3084. [CrossRef]
6. Ran, H.; Yu, Q.; Qin, K.; Zhao, Q.; Zeng, X. Experimental study of truss reinforced concrete laminated slabs in service phase. *Struct. Eng.* **2019**, *35*, 164–171. (In Chinese)
7. Li, J.; Huang, H.; Zeng, C.; Zhang, M.; Huang, S. A simplified elastic calculation method for four-sided solidly supported precast ribbed bottom concrete two-way laminated slabs. *J. Hunan Univ. Sci. Technol. (Nat. Sci. Ed.)* **2020**, *35*, 33–43. (In Chinese)
8. Jiang, D.; Huang, H.; Zhu, M.; Zhang, M.; Huang, S. Experimental study on flexural fatigue performance of precast prestressed ribbed base concrete laminated slabs. *Ind. Constr.* **2020**, *50*, 76–83.
9. Huang, H.; Wu, F.; Zhu, M.; Zeng, C.; Lv, W. Study on the influence of plate rib form on the flexural performance of precast ribbed bottom concrete laminated slabs. *J. Build. Struct.* **2015**, *36*, 66–72. (In Chinese)
10. An, H.; Zheng, Z.; Cao, Y.; Li, X.; Wang, W. Experimental study on flexural performance of reinforced truss fiber cement composite slabs. *Build. Struct.* **2022**, *52*, 74–78+131. (In Chinese)
11. Huang, H.; Zhou, P.; Zhang, M.; Gao, Y. Simplified plastic design method of prefabricated composite rib concrete two-way superimposed slab cross beam floor. *Build. Struct.* **2022**, *52* (Suppl. S1), 1738–1743. (In Chinese)
12. Liu, Y. Study on the Performance of Self-Supporting Reinforced Truss Concrete Laminated Slabs. Master's Thesis, Zhejiang University, Hangzhou, China, 2006. (In Chinese)

13. Ma, L.; Chen, X.; Jiang, L.; Yu, Z.; Zhang, Z. Experimental and finite element analysis of reinforced truss concrete laminated floor slabs. *Build. Struct.* **2013**, *43*, 54–57+62. (In Chinese)

14. Zhao, L. Research on the Design and Calculation Method of Self-Supporting Reinforced Truss Concrete Laminated Slab. Master's Thesis, Central South University, Changsha, China, 2007. (In Chinese)

15. Cheng, J.Y.; Lei, Z.; Jian, J.Y. Study on short term rigidity of precast composite slab with steel truss and concrete. In *Advanced Materials Research*; Trans Tech Publications Ltd.: Wollerau, Switzerland, 2013; Volume 639.

16. Wu, F.; Huang, H.; Chen, W.; Zhou, X. Experimental study on the force performance of prefabricated ribbed thin concrete laminated slabs. *Civ. Constr. Environ. Eng.* **2011**, *33*, 7–12+19. (In Chinese)

17. Qian, H.; Zhou, K. Experimental study of PK prestressed concrete laminated slabs. *Chin. Foreign Archit.* **2006**, *3*, 96–97.

18. Shi, L.; Wang, H.; Wang, Q.; Li, X. Analysis of mechanical properties of prestressed ribbed concrete laminated slabs. *Build. Struct.* **2021**, *51* (Suppl. S1), 1135–1141. (In Chinese)

19. Huang, W.; Ma, X.; Luo, B.; Li, Z.; Sun, Y. Experimental study on flexural behaviour of lightweight multi-ribbed composite slabs. *Adv. Civ. Eng.* **2019**, *1*, 1–11. [CrossRef]

20. Li, M.; Wang, H.; Zhao, W. Testing the force performance of unidirectional laminated plates with shear keys. *J. Jilin Univ. (Eng. Ed.)* **2020**, *50*, 654–667. (In Chinese)

21. Li, M.; Wang, H.; Zhao, W. Mechanical properties and design methods of unidirectional laminated plates with shear bonds. *J. Build. Sci. Eng.* **2019**, *36*, 35–45. (In Chinese)

22. *JGJ1-2014*; Technical Specification for Precast Concrete Structures. Ministry of Housing and Urban-Rural Development of the People's Republic of China: Beijing, China; Architecture & Building Press: Beijing, China, 2014. (In Chinese)

23. Li, X.; Yin, J.; Xu, Q. Experimental research on mechanical properties of RC two-way cast-in-situ slab with existing cracks. *Earthq. Resist. Eng. Retrofit.* **2010**, *32*, 47–51. (In Chinese)

24. Du, X.; Dang, L.; Ren, Q. Plastic damage cracking study on the reinforced concrete slab. *Water Power* **2009**, *35*, 28–29+56. (In Chinese)

25. Ma, T. Study on Hybrid Testing of Continuous Beambridge Structure Based on Bilinear Model Renewal. Master's Thesis, Suzhou University of Science and Technology, Suzhou, China, 2019. (In Chinese)